

Cathodic Phase Transformations During Direct Electrolytic Reduction of Nb₂O₅ in a CaCl₂-NaCl-CaO Melt

Qiu-shi Song, Qian Xu^{*}, Ran Tao, Xue Kang

School of Materials Science and Metallurgy, Northeastern University, Shenyang, 110819, P R China.

*E-mail: qianxu201@mail.neu.edu.cn

Received: 25 September 2011 / Accepted: 27 November 2011 / Published: 1 January 2012

The phase transformations during direct electrochemical reduction of Nb₂O₅ were investigated through constant potential electrolysis in a CaCl₂-NaCl-CaO melt at 1073 K. The microstructure and phase compositions of the cathode during the reduction were determined. The mechanism of the transformations was elucidated in the view of structure. The results show Chemical reactions between CaO and Nb₂O₅ occurred spontaneously in the melt, forming calcium niobates with different morphology. During the electrodeoxidation, the intercalation of calcium ions into the cathode formed calcium niobates with large particle size, and then disintegrated them to much smaller ones. The CaO concentration in the CaCl₂-NaCl melt can affect the morphology of final niobium product.

Keywords: electrochemical reduction; niobium; calcium oxide; calcium niobate; phase transformation

1. INTRODUCTION

In recent years, a novel metallurgical process to obtain metals and alloys through direct electrochemical reduction of the respective oxides in molten salts has been widely investigated [1-22]. As a promising method to produce niobium in a simpler and more environmentally friendly way [7, 23, 24], it has been reported from many aspects such as optimizing the experimental conditions and pursuing the reaction mechanism. Yan et al. proposed a conceptual model with a number of key parameters considered, and depicted the cathodic process in electro-deoxidation of solid Nb₂O₅ in CaCl₂-NaCl melt [3, 14, 20, 21]. Qiu et al. investigated the electrochemical reduction process of Nb₂O₅ powder with metallic cavity electrode [4]. Xu et al. improved the fabrication of the cathode by adding CaO and CaCO₃ into the Nb₂O₅ [5]. Wang et al. investigated the reduction process from the aspect of electrochemical analysis [25]. Kar et al. applied some models to understand the electro-deoxidation process [26, 27].

From previous studies, calcium niobates of $\text{Nb}_2\text{O}_5 \cdot n\text{CaO}$ ($n=1, 2, 3$) were usually observed when the electro-deoxidation of Nb_2O_5 was carried out in CaCl_2 or CaCl_2 -based melts [3-6, 20, 21]. Though the calcium niobates could be subsequently reduced to sub-oxides of niobium, the effect of CaO on the reduction process seemed to be unclear. Actually, the formation of calcium-enriched oxides have also been observed during the electro-deoxidation of some other metallic oxides, such as TiO_2 [11, 12, 28, 29], Ta_2O_5 [7-9, 22] and Cr_2O_3 [30, 31]. All the results reveal that CaO plays an important role in the electrochemical reduction process.

The objective of this work has been to gain a great insight into the phase and microstructure transformations during the electrochemical reduction of Nb_2O_5 in a CaCl_2 - NaCl melt containing CaO . It is intended to investigate the reduction pathway of Nb_2O_5 in the melt and the behavior of CaO during the electro-deoxidation, in order to better understand the mechanism of Nb_2O_5 reduction, which may be critical for successful industrialization.

2. EXPERIMENTAL

All chemicals in this study were of analytical grade. Nb_2O_5 powder (99.99% in purity) was weighted 1.0g and compacted into cylindrical pellets under 12MPa, which were then sintered at 1273K for 12h. A eutectic mixture of CaCl_2 and NaCl was melted in an alumina crucible, and then 1mol% of CaO was added into the molten salt, which served as the electrolyte. The sintered oxide pellet was immersed in the melt as the cathode. High-density graphite rods of 12 mm diameter and 70 mm length served as the anodes. The experimental apparatus utilized in this work were similar to those described in the literature [5, 8, 9, 19, 22]. All the electrochemical experiments were carried out under an atmosphere of dried argon.

A constant voltage of 2.8V was applied between the cathode and anode at 1073K. In order to obtain incompletely and completely reduced specimens, the electrolysis was terminated after various reaction times ranging from 0.5 to 13.5h. The samples were removed from the melt and cooled down to room temperature, which were vigorously rinsed with tap water and dried for examination. To investigate chemical interaction between CaO and Nb_2O_5 , the sintered pellets were immersed into the molten salt without a voltage applied. Phase composition of all the samples was determined through a D/Max-2500PC X-ray diffractometer with $\text{Cu-K}\alpha$ radiation (XRD). Morphology and chemical composition of the samples were investigated by means of a SSX-550 scanning electron microscope (SEM) equipped with energy-dispersive X-ray analysis (EDX).

3. RESULTS AND DISCUSSION

The sintered Nb_2O_5 pellet has been characterized by SEM, as shown in Fig. 1a, which contains particles of about 1-5 μm in diameter. But morphology of particles changed greatly when the sintered pellet was immersed in the melt for 6h without the application of a voltage. Fig. 1b shows the cross section morphology of the immersed pellet, whose particle size decreases from the outer surface to the

central part of the pellet. The outer surface of the sample (A in Fig. 1c) consists of wirelike particles with a high aspect ratio, which reach over 50 μm in length and present obvious preferential orientation. Then a layer of rodlike particles (B in Fig. 1c) can be observed adjacent to wirelike ones, which are much coarser and have a length of less than 10 μm . And the preferential orientation is less visible. Then, the lath-shaped particles (C and D in Figs. 1d-e) exist in the interior region of the pellet, which exceed more than 100 μm . However, the particles in the central part of the sample (E in Fig. 1f) seem to be similar to those of the sintered pellet (in Fig. 1a), which are less than 10 μm .

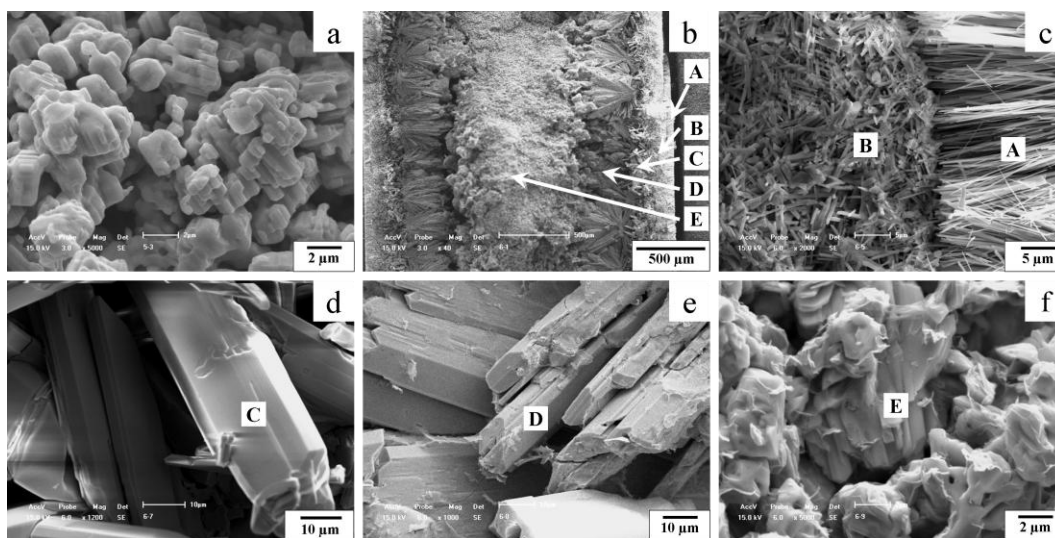


Figure 1. SEM images of (a) the Nb₂O₅ sintered pellet at 1273K for 12h; (b) the cross section of the sample immersed in the CaCl₂-NaCl-1mol% CaO melt for 6h; (c)~(f) The enlarged images of different types of particles in the sample immersed in the melt for 6h.

Table 1. The molar ratios of Ca to Nb for the sample in Figs. 1c-f, respectively.

Region	Ca:Nb
A	0.61:1
B	0.4:1
C	0.39:1
D	0.42:1
E	0.28:1

According to the respective EDX analyses presented in Table 1, the calcium to niobium ratio decreases from the surface to the central parts of the pellet. Furthermore, the XRD pattern of the pellet in Fig. 2 exhibits predominantly peaks for Nb₂O₅·CaO and Nb₂O₅·2CaO. All the results indicate the formation of calcium niobates. Actually, the chemical reactions between Nb₂O₅ and CaO have already been reported [4, 20, 21], and calcium niobates, basically Nb₂O₅·CaO, can be found on surface of the Nb₂O₅ sample. But the results above show that calcium niobates with various compositions can be

formed. And the morphology of particles in the pellet is also associated with their chemical compositions.

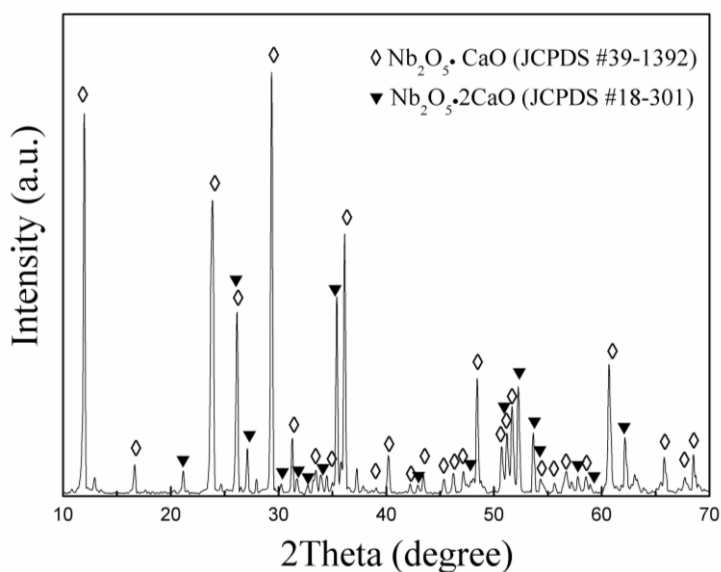


Figure 2. XRD pattern of the sample immersed in the CaCl₂-NaCl-1mol% CaO melt for 6h.

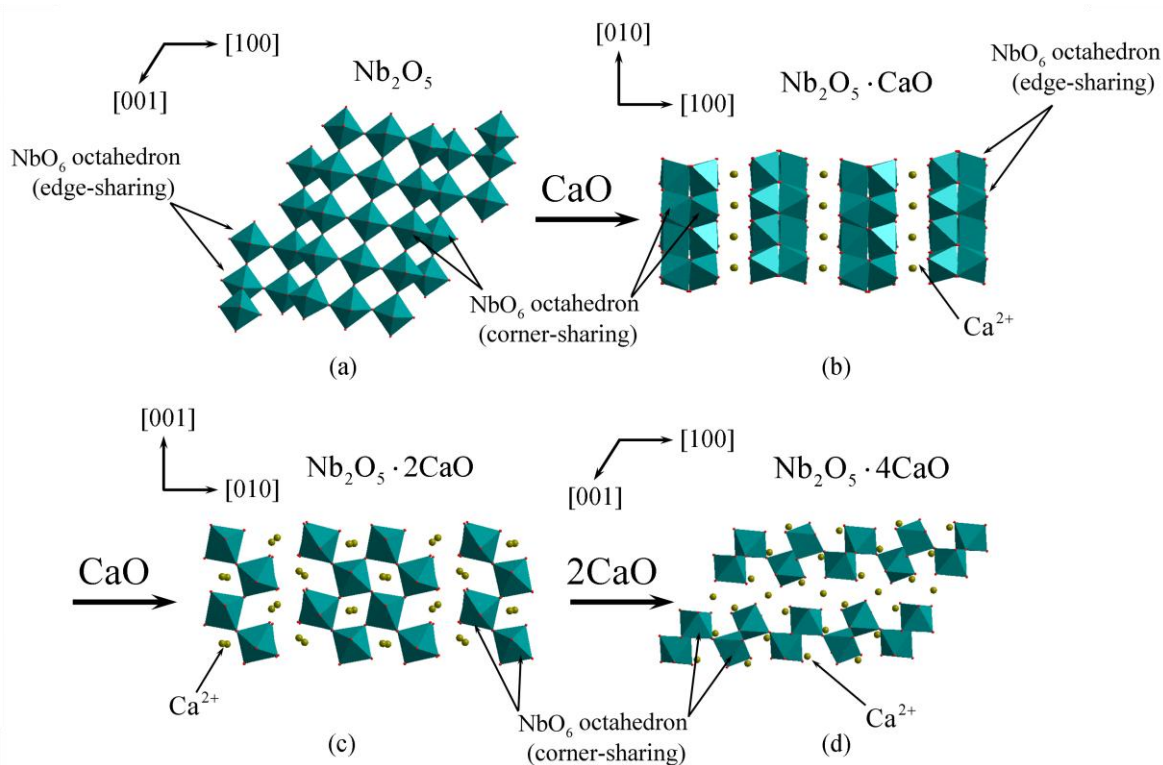


Figure 3. Schematic illustration of the structural transformations of calcium niobates in the CaCl₂-NaCl-1mol% CaO melt.

The formation of calcium niobates is probably related with the concentration of CaO in the melt. More CaO were combined on the surface of the immersed pellet, where its concentration was relative higher because of the diffusion of CaO through the channels of open porosity in the sample. However, the percolation of CaO was less effective in the inner part of the oxide pellet, so calcium niobates containing less CaO were formed due to the relative lower concentration of CaO. In the center of the sample, the calcium to niobium ratio was the lowest one, where the particles were similar to those in the sintered pellet. As a result, calcium niobates with various compositions are formed across the pellet.

From the point of the view of structure, the transformation of the particles morphology during the chemical reactions is discussed. Nb_2O_5 has atomic structure formed from corner-sharing and edge-sharing NbO_6 octahedra, as illustrated in Fig. 3a. When the sintered pellet was immersed into the molten salt, Nb_2O_5 would combine CaO in the melt. O^{2-} ions went to the NbO_6 octahedron arrays, and Ca^{2+} ions were located in interstitial sites among NbO_6 octahedra. The amount of bridging oxygen linking the NbO_6 octahedra decreased, and more non-bridging oxygen were formed at the same time. So the Nb-O network of Nb_2O_5 was changed to a stacking of Nb-O sheets consisting of corner-sharing and edge-sharing NbO_6 octahedra, and layers of Ca^{2+} ions between the Nb-O sheets in the structure of $\text{Nb}_2\text{O}_5 \cdot \text{CaO}$ in Fig. 3b. The process of bond-breaking, rebonding and new generation of bonds provides a chance for initial particles of Nb_2O_5 to grow to much bigger ones, as illustrated in Figs. 1d and e. As more Ca^{2+} and O^{2-} ions were intercalated into the pellet, the connection between the edge-sharing NbO_6 octahedra was broken up, and Ca^{2+} ions was located in the tunnel space of the Nb-O sheets at the same time, as shown in the structure of $\text{Nb}_2\text{O}_5 \cdot 2\text{CaO}$ in Fig. 3c. Fig. 3d reveals that Ca^{2+} ions in the tunnel space transformed to layered space by further breaking up of bridging oxygen when $\text{Nb}_2\text{O}_5 \cdot 4\text{CaO}$ was formed. In the process above, the Nb-O network with higher polymerization of NbO_6 octahedra was decomposed to the network with lower polymerization of NbO_6 octahedra, which would disintegrate the larger, lath-shaped particles into much smaller ones. CaO behaved here as a network modifier, and its disagglomeration effect towards the particles is more obvious with increasing amount of CaO incorporated into the pellets.

Figs. 4a-c show the XRD patterns of partially reduced samples for 0.5, 1 and 2h, respectively. $\text{Nb}_2\text{O}_5 \cdot \text{CaO}$ and $\text{Nb}_2\text{O}_5 \cdot 2\text{CaO}$ were detected in the sample after 0.5h of reduction. It means the chemical reactions between Nb_2O_5 and CaO have occurred. Meanwhile, electro-deoxidation of niobium oxides have taken place, since the electrons had already been supplied to the cathode, which can be confirmed by the appearance of NbO_2 and $\text{Nb}_2\text{O}_3 \cdot \text{CaO}$. The appearance of $\text{Nb}_2\text{O}_3 \cdot \text{CaO}$ means that lower-valency niobium oxides can also react with CaO. In the sample quenched after reduction for 1h, $\text{Nb}_2\text{O}_3 \cdot \text{CaO}$ had already transformed to $\text{Nb}_2\text{O}_5 \cdot 2\text{CaO}$. When the reduction time was prolonged to 2h, $\text{Nb}_2\text{O}_5 \cdot 3\text{CaO}$ and $\text{Nb}_2\text{O}_5 \cdot 4\text{CaO}$, which were not observed in the sample maintained in the melt without the application of a voltage, were found besides the further reduction product of niobium. CaCO_3 can also be detected because of the generation of carbon dioxide on the anode during electrolysis. The results above shows that the formation of calcium niobates occurs during the electro-deoxidation. Nb_2O_5 could combine more CaO, compared with the results without an application of a voltage. When the electro-deoxidation began, the release of oxygen ions from cathode to the melt would increase the concentration of CaO around the cathode as discussed in previous studies [22], and

it also raised the quantity of oxygen voids in the crystal structure of the cathode. This process would enable further combination of CaO into the cathode.

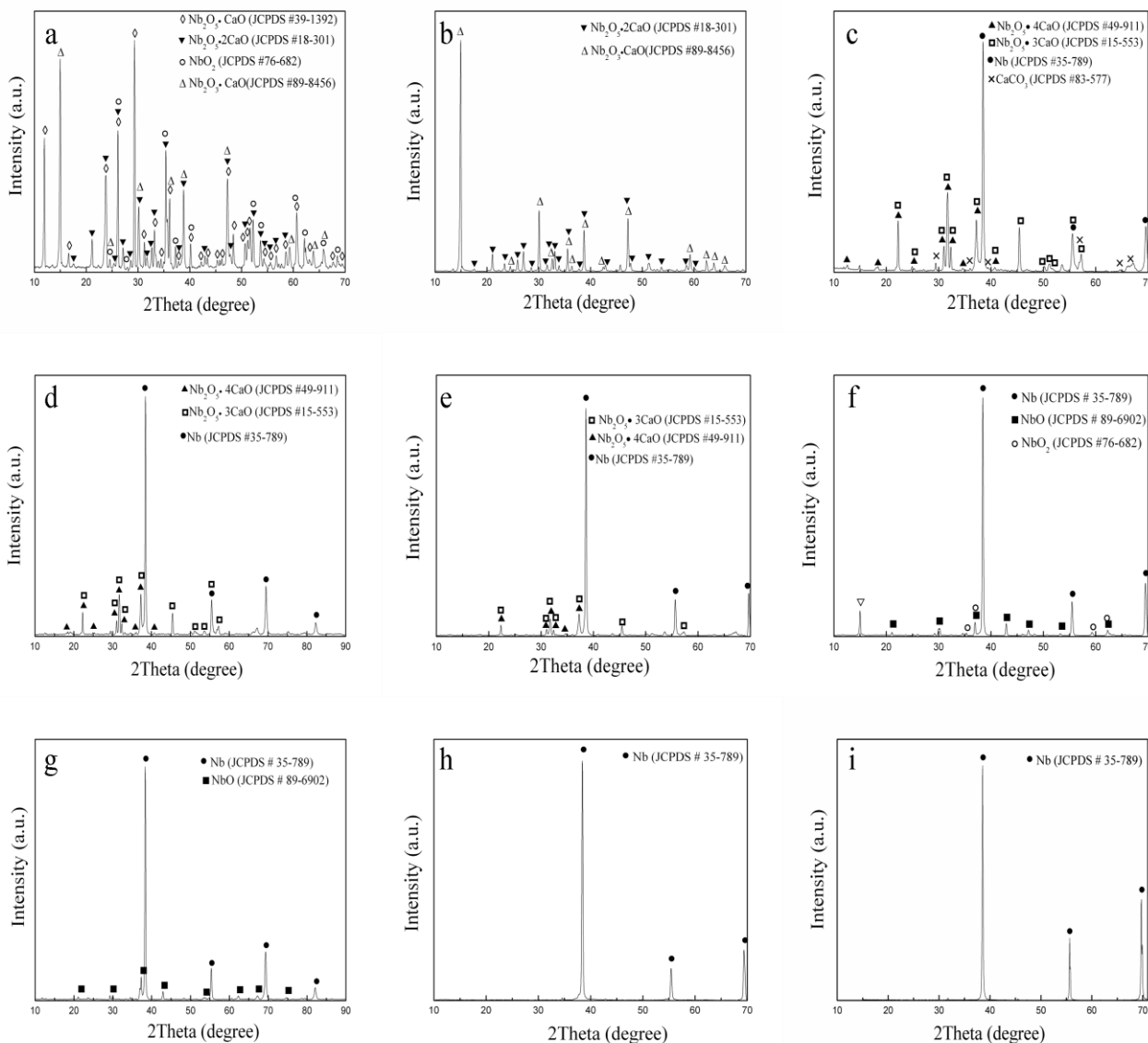


Figure 4. XRD patterns of the samples electro-deoxidized in the $\text{CaCl}_2\text{-NaCl-1mol\% CaO}$ melt for (a) 0.5h, (b) 1h, (c) 2h, (d) 5h, (e) 7.5h, (f) 10h, (g) 12h, (h) 13.5h, respectively; (i) XRD pattern of the sample electro-deoxidized in the $\text{CaCl}_2\text{-NaCl}$ melt without an addition of CaO for 8h at 1073K.

Fig. 5a is SEM image of the partially reduced sample for 0.5h. There are several types of particles classified by their sizes. According to the respective EDX analysis in Table 2, no calcium is contained in region F, which indicates NbO_2 from the reduction of Nb_2O_5 ; the molar ratios of Ca to Nb for regions G and H are 0.46:1 and 0.39:1, respectively, where the major phase is $\text{Nb}_2\text{O}_5 \cdot \text{CaO}$; while the ratio for region I is 0.68:1, the major phases are $\text{Nb}_2\text{O}_5 \cdot \text{CaO}$, $\text{Nb}_2\text{O}_5 \cdot 2\text{CaO}$ and $\text{Nb}_2\text{O}_3 \cdot 2\text{CaO}$,

confirmed by the XRD analysis. Fig. 5b shows the morphology of the partially reduced sample for 1h. The EDX analysis for regions J and K is 0.86:1 and 0.74:1, respectively, where the major phases may be $\text{Nb}_2\text{O}_5 \cdot 2\text{CaO}$ and $\text{Nb}_2\text{O}_3 \cdot 2\text{CaO}$. Fig. 5c presents the morphology of sample after 2h of reduction, and EDX analysis was carried out for the regions marked by L and M. The mole ratio of Ca to Nb for region is 4:1, where the major phase is Nb, $\text{Nb}_2\text{O}_5 \cdot 3\text{CaO}$ and $\text{Nb}_2\text{O}_5 \cdot 4\text{CaO}$ from the XRD analysis; and the ratio for region M is 0.09:1, where the major phase is Nb because of the small amount of Ca and its XRD pattern. From the SEM and EDX results of the partially reduced samples for 0.5, 1 and 2h, it reveals that the intercalation of CaO into the cathode has great influence on its morphology. The particles in the cathode changed to much bigger ones at the initial incorporation of CaO as shown by regions G and H in Fig. 5a, which is similar with that during the immersion of Nb_2O_5 into the melt without an application of a voltage. This may be a challenge for the electro-deoxidation because of the increased diffusion distance for oxygen ions from the cathode to the melt. However, the further incorporation of CaO into the cathode would decompose the particles to smaller ones, as illustrated by region J in Fig. 5b, which reflects the aggregation of the smaller flakes. When $\text{Nb}_2\text{O}_5 \cdot 3\text{CaO}$ and $\text{Nb}_2\text{O}_5 \cdot 4\text{CaO}$ are formed, the size of most particles in the sample is smaller than $5\mu\text{m}$, as shown in Fig. 5c.

Table 2. The molar ratios of Ca to Nb for the samples in Figs. 4a-c, respectively.

Region	Ca:Nb	Region	Ca:Nb
F	0:1	J	0.86: 1
G	0.46:1	K	0.74:1
H	0.39:1	L	4: 1
I	0.68:1	M	0.09:1

Figs. 4d-e are the XRD patterns of the partially reduced for 5h and 7.5h, respectively. The major phase is Nb, and the minor phases are $\text{Nb}_2\text{O}_5 \cdot 3\text{CaO}$ and $\text{Nb}_2\text{O}_5 \cdot 4\text{CaO}$. The CaO incorporated into the cathode seems to be saturated when $\text{Nb}_2\text{O}_5 \cdot 4\text{CaO}$ was formed. It means that the stable structure of the Nb-O network would be destroyed if $\text{Nb}_2\text{O}_5 \cdot 4\text{CaO}$ connected with corner-sharing NbO_6 octahedra combined more CaO. Moreover, the characteristic peaks of $\text{Nb}_2\text{O}_5 \cdot 3\text{CaO}$ and $\text{Nb}_2\text{O}_5 \cdot 4\text{CaO}$ gradually disappear with the increasing of reduction time, which means the calcium niobates have been further reduced to Nb. According to the SEM images of the samples in Fig. 5d-e, the particle sizes are smaller than those after 2h of reduction. Figs. 4f-g are XRD patterns of the samples reduced for 10 and 12h. Sample recovered for 10h mainly contains NbO_2 , NbO and Nb. It implies that calcium niobates have already been consumed after 10h of reduction. Then NbO_2 was reduced to NbO after 12h of reduction. Figs. 5g-h present morphology of the sample reduced for 10 and 12h. The particles are smaller than those of calcium niobates, and some of them are interconnected one another. But the particle size is not uniform probably because incomplete reduction of the samples and the niobium oxides particle size may be bigger.

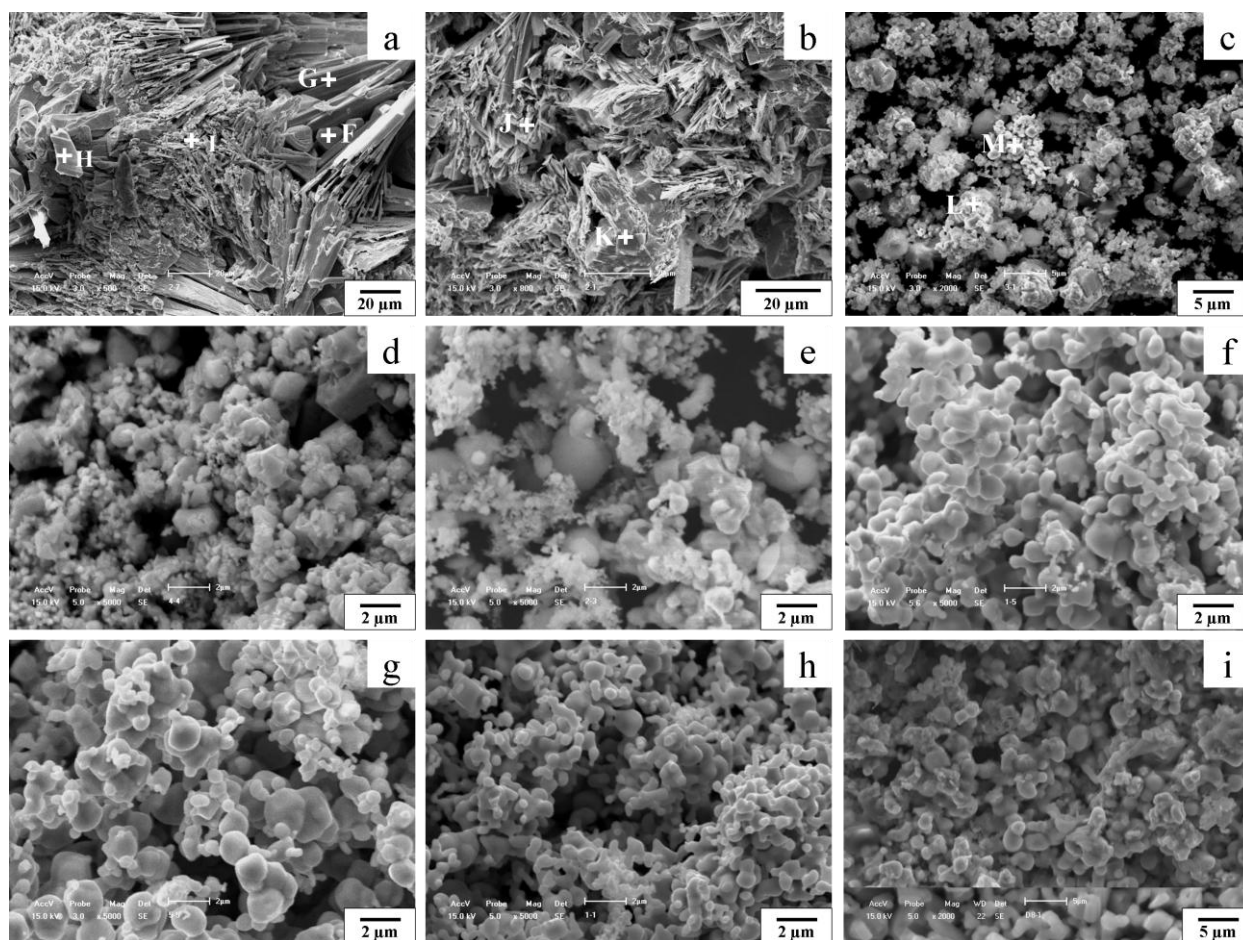


Figure 5. SEM images of the samples electro-deoxidized in the $\text{CaCl}_2\text{-NaCl-1mol\% CaO}$ melt for (a) 0.5h, (b) 1h, (c) 2h, (d) 5h, (e) 7.5h, (f) 10h, and (g) 12h, (h) 13.5h, respectively; (i) SEM image of the sample electro-deoxidized in the $\text{CaCl}_2\text{-NaCl}$ melt without an addition of CaO for 8h at 1073K.

Fig. 4h shows XRD pattern of the sample reduced for 13h, in which metallic niobium is the only phase being present, indicating completely reduction of the cathode. And its morphology is presented in Fig. 5h. It presents uniform particle sizes and similar interconnected nodular shapes of the metal niobium product. Compared with the morphology of particles obtained in eutectic $\text{CaCl}_2\text{-NaCl}$ melt without the addition of CaO in Fig. 5i, they are smaller, and have smoother surface, though the XRD pattern shows that the two kinds of particles are both niobium, as illustrated in Fig. 4h-i. It informs that the morphology of the final product can probably be modified by controlling the concentration of CaO in the melt. This finding is in accordance with the results in the process of calciothermic reduction of Ta_2O_5 in the molten CaCl_2 by Suzuki et al [32, 33].

Fig. 6 is the current vs. time curve, which was recorded during 13.5h of electrochemical reduction of Nb_2O_5 in the $\text{CaCl}_2\text{-NaCl-1mol\%CaO}$ melt. The plot commences with a current peak that extends over about 1h, which is followed by a current shoulder that spans over about 2h. The current peak is caused by fast reductions of the cathode with participation of calcium oxide as indicated by $\text{Nb}_2\text{O}_5\cdot\text{CaO}$ and $\text{Nb}_2\text{O}_5\cdot 2\text{CaO}$ in Fig. 4a, which lead to the formation of calcium niobates. Though the decay of current is slower with further incorporation of CaO to form $\text{Nb}_2\text{O}_5\cdot 4\text{CaO}$, it remains a high

value during about 1-3h reduction illustrated by the current shoulder, which means relatively faster reduction of the cathode. Thereafter the current gradually drops slowly to a relatively smaller value during about 3-8h of reduction, in which calcium niobates formation seems to cease and the removal of oxygen from the cathode becomes the dominant process. During the later stages of the reduction process, the oxygen content in the cathode is low for the formation of the major phase of niobium and the minor phase of niobium oxides, as shown in Fig. 4f-g, so the electronic current now contributes significantly to the overall current. This probably leads the relatively low overall current efficiency for preparation of niobium.

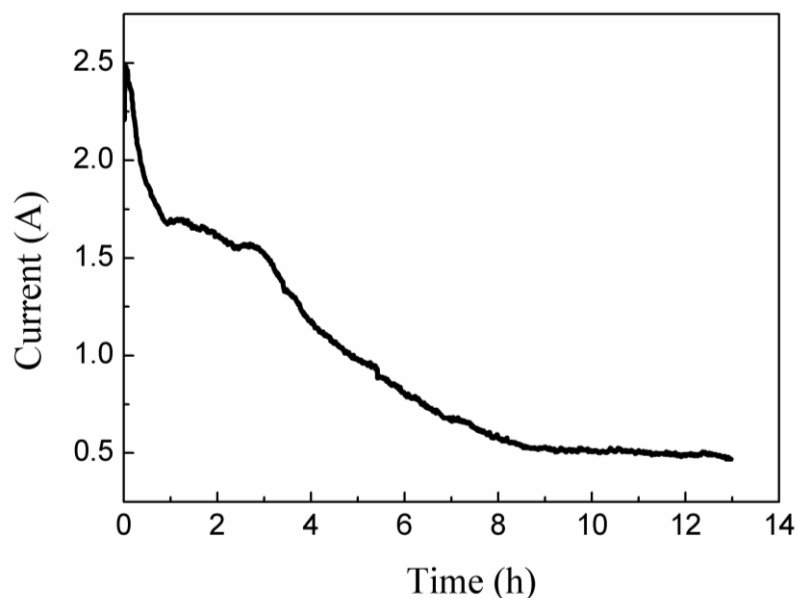


Figure 6. The current vs. time curve of electrochemical reduction of Nb_2O_5 for 13.5h in the $\text{CaCl}_2\text{-NaCl-1mol\% CaO}$ melt.

4. CONCLUSIONS

Nb_2O_5 were reduced electrochemically and to different extents under a voltage of 2.8 V in molten $\text{CaCl}_2\text{-NaCl-1mol\%CaO}$ at 1073K. The transformations of cathode and the behavior of CaO during of electro-deoxidization are investigated. CaO in the melt can react chemically with Nb_2O_5 in the melt, and change morphology of the sintered pellet by forming calcium niobates of $\text{Nb}_2\text{O}_5 \cdot n\text{CaO}$ ($n=1, 2, 3, 4$) with various morphology, depending on the concentration of CaO in the molten salt. During the electrochemical reduction process from Nb_2O_5 to Nb, the cathode undergoes further intercalation of CaO to form calcium niobates, which disintegrate calcium niobates with bigger particle size to those with smaller particle size. The calcium niobates are subsequently reduced to niobium oxides, and finally metallic niobium. The addition of CaO into the melt can assist the removal of the oxygen ions from the cathode by forming calcium niobates with small particle size, but lower current

efficiency of the later stage from niobium suboxides to niobium. Furthermore, the bulk concentration of CaO in the melt can affect the particle size of the final Nb product.

ACKNOWLEDGMENTS

The authors acknowledge the National Natural Science Foundation of China (Grant No. 50574025 and 50874026), the Natural Science Foundation of Liaoning Province (Grant No.20062020), China, and the Doctoral Dissertation Foundation of Northeastern University, China for financial supports.

References

1. G.Z. Chen, D.J. Fray and T.W. Farthing, *Nature*, 407 (2000) 361.
2. D.J. Fray, T.W. Farthing and G.Z. Chen, *International Patent* PCT/GB99/01781.
3. X.Y. Yan and D.J. Fray, *Metall. Mater. Trans. B*, 33B (2002) 685.
4. G.H. Qiu, D.H. Wang, X.B. Jin and G.Z. Chen, *Electrochim. Acta*, 51 (2006) 5785.
5. Q. Xu, L.Q. Deng, Y. Wu and T. Ma, *J. Alloys Compd.*, 396 (2005) 288.
6. T. Wu, W. Xiao, X.B. Jin, C. Liu, D.H. Wang and G.Z. Chen, *Phys. Chem.*, 10 (2008) 1809.
7. T. Wu, X.B. Jin, W. Xiao, X.H. Hu, D.H. Wang and G.Z. Chen, *Chem. Mater.*, 19 (2007) 153.
8. X.F. Hu and Q. Xu, *Acta Metall. Sinica*, 42 (2006) 285.
9. X.F. Hu, Q. Xu and Y. Wu, *Mater. Rev.*, 19 (2005) 97.
10. C. Schwandt and D.J. Fray, *Electrochim. Acta*, 51 (2005) 66.
11. D.T.L. Alexander, C. Schwandt and D.J. Fray, *Acta Mater.*, 54 (2006) 2933.
12. C. Schwandt, D.T.L. Alexander and D.J. Fray, *Electrochim. Acta*, 54 (2009) 3819.
13. X.Y. Yan and D.J. Fray, *Adv. Funct. Mater.*, 15 (2005) 1757.
14. X.Y. Yan, D.J. Fray, *J. Appl. Electrochem.* 39 (2009) 1349.
15. B. Jackson, M. Jackson, D. Dye and D. Inman, *J. Electrochem. Soc.*, 155 (2008) E171.
16. S. Tan, T. Oers, M.K. Aydinol, T. Ozturk and I. Karakaya, *J. Alloys Compd.*, 475 (2009) 368.
17. B.J. Zhao, L. Wang, L. Dai, G.H. Cui, H.H. Zhou and R.V. Kumar, *J. Alloys Compd.*, 468 (2009) 379.
18. Y. Zhu, D.H. Wang, M. Ma, X.H. Hu, X.B. Jin and G.Z. Chen, *Chem. Commun.*, 24 (2007) 2515.
19. X. Kang, Q. Xu, S.J. Ma, L.N. Zhao and Q.S. Song, *Electrochemistry*, 77 (2009) 663.
20. X.Y. Yan and D.J. Fray, *J. Electrochem. Soc.*, 152 (2005) D12.
21. X.Y. Yan and D.J. Fray, *J. Electrochem. Soc.*, 152 (2005) E308.
22. Q.S. Song, Q. Xu, X. Kang, J.H. Du and Z.P. Xi, *J. Alloys Compd.*, 490 (2010) 24.
23. I. Park, T.H. Okabe and Y. Waseda, *J. Alloys Compd.*, 280 (1998) 265.
24. S.M. Jeong, H.Y. Yoo, J.M. Hur and C.S. Seo, *J. Alloys Compd.*, 440 (2007) 210.
25. S.L. Wang, Y. Xue and H. Sun, *J. Electroanal. Chem.*, 595 (2005) 109.
26. P. Kar and J.W. Evans, *Electrochim. Acta*, 53 (2008) 5260.
27. P. Kar, *J. Solid State Electrochem.*, 12 (2008) 161.
28. K. Jiang, X.H. Hu, M. Ma, D.H. Wang, G.H. Qiu, X.B. Jin and G.Z. Chen, *Angew. Chem. Int. Ed.*, 45 (2006) 428.
29. G.Z. Chen and D.J. Fray, *J. Electrochem. Soc.*, 149 (2002) E455.
30. G.Z. Chen, E. Gordo and D.J. Fray, *Metall. Mater. Trans. B*, 35B (2004) 223.
31. C. Schwandt and D. J. Fray, *Z. Naturforsch. A*, 62 (2007) 65.
32. M. Baba and R.O. Suzuki, *J. Alloys Compd.*, 392 (2005) 225.
33. R.O. Suzuki, M. Baba, Y. Ono and K. Yamamoto, *J. Alloys Compd.*, 389 (2005) 310.